Development Advance Online Articles. First posted online on 7 March 2016 as 10.1242/dev.132654
Access the most recent version at http://dev.biologists.org/lookup/doi/10.1242/dev.132654

Clarification of mural cell coverage of vascular endothelial cells by live imaging of zebrafish

Koji Ando[1], Shigetomo Fukuhara[1*], Nanae Izumi[2], Hiroyuki Nakajima[1], Hajime Fukui[1], Robert N. Kelsh[3] and Naoki Mochizuki[1,4*]

[1]Department of Cell Biology, National Cerebral and Cardiovascular Center Research Institute, 5-7-1 Fujishirodai, Suita, Osaka 565-8565, Japan

[2]Frontier Research Laboratories, R&D Division, Daiichi Sankyo Co., Ltd., 1-2-58, Hiromachi, Shinagawa-ku, Tokyo 140-8710, Japan

[3]Centre for Regenerative Medicine, Developmental Biology Programme, Department of Biology and Biochemistry, University of Bath, Bath BA2 7AY, UK

[4]AMED-CREST. National Cerebral and Cardiovascular Center, 5-7-1, Suita, Osaka 565-8565, Japan

Key Words: Mural cells, Pericytes, Vascular smooth muscle cells, Zebrafish, pdgfrb

Summary: Live-imaging of mural cell dynamics in zebrafish uncovers the mechanism how the mural cells develop and cover the endothelial cells during vascular development.

***To whom correspondence should be addressed**

Shigetomo Fukuhara: fuku@ncvc.go.jp

Naoki Mochizuki: nmochizu@ncvc.go.jp

Address: Department of Cell Biology, National Cerebral and Cardiovascular Center Research Institute, 5-7-1 Fujishirodai, Suita, Osaka 565-8565, Japan

Tel.: +81-6-6833-5012; Fax: +81-6-6835-5461

ABSTRACT

Mural cells (MCs) consisting of vascular smooth muscle cells and pericytes cover the endothelial cells (ECs) to regulate vascular stability and homeostasis. Here, we clarified the mechanism how MCs develop and cover ECs by generating the transgenic zebrafish lines that allow live imaging of MCs and by lineage tracing *in vivo*. To cover cranial vessels, MCs derived from either neural crest cells or mesoderm emerged around the preformed EC tubes, proliferated and migrated along EC tubes. During their migration, the MCs moved forward by extending their processes along the inter-EC junctions, suggesting the role of inter-EC junctions as a scaffold for MC migration. In the trunk vasculature, MCs derived from mesoderm covered the ventral side of the dorsal aorta (DA), but not the posterior cardinal vein. Furthermore, the MCs migrating from the DA or emerging around intersegmental vessels (ISV) preferentially covered arterial ISVs rather than venous ISVs, indicating that MCs mostly cover arteries during vascular development. Thus, live imaging and lineage tracing enabled us to precisely clarify how MCs cover the EC tubes and to identify the origins of MCs.

INTRODUCTION

The vasculature consists of two principle cell types: endothelial cells (ECs) and mural cells (MCs). The ECs line the inner surface of the blood vessels, while the MCs cover the abluminal surface of the ECs. The MCs are further classified into two types, vascular smooth muscle cells (VSMCs) and pericytes (Gaengel et al., 2009). The former consist of multi-layered cells and ensheath ECs, whereas the latter are solitary cells associated with the small diameter blood vessels such as arterioles, venules and capillaries. The MCs play an essential role in vascular stability and homeostasis (Armulik et al., 2011). Therefore, loss or detachment of the MCs leads to various vascular diseases (French et al., 2014; Garg et al., 2014; Joutel et al., 1996).

The MCs originate from distinct developmental precursors such as mesoderm-derived mesenchymal cells and neural crest cells (Majesky, 2007; Wasteson et al., 2008; Winkler et al., 2011). These precursors are thought to be recruited to the vessel wall and to differentiate into the MCs, which subsequently proliferate and migrate to cover the entire vessels (Armulik et al., 2011; Hellstrom et al., 1999). However, when and how the progenitor cells differentiate into the MCs and cover the blood vessels during vascular development remains still largely unknown, because no clear methods for analyzing MCs in living animals have been developed. To date, although the zebrafish transgenic (Tg) lines such as *Tg(sm22a-b:GFP)* and *Tg(acta2:EGFP)* have been developed to visualize the MCs *in vivo* (Seiler et al., 2010; Whitesell et al., 2014), only limited parts of vasculature were covered by perivascular EGFP-expressing cells in these Tg zebrafish lines. Thus, these fish lines may not faithfully report all MCs *in vivo*.

Platelet-derived growth factor (PDGF)-B/PDGF receptor β (PDGFRβ) signaling pathway plays a crucial role in the regulation of MC coverage of blood vessels (Hellstrom

et al., 1999; Olson and Soriano, 2011a; Wang et al., 2014). PDGF-B secreted from the ECs binds to PDGFRβ receptors expressed on the MCs, thereby promoting recruitment of MCs and subsequent their proliferation and migration. Recently, Wang et al. successfully visualized pericytes covering cerebral vessels in the zebrafish brain by performing fluorescence *in situ* hybridization (ISH) for *pdgfrb* (Wang et al., 2014). However, this method does not allow the analysis of MC dynamics *in vivo*.

Here, we have succeeded in visualizing the MCs in living zebrafish by developing Tg lines in which EGFP, mCherry or Gal4FF driver, an engineered transcriptional activator consisting of the DNA-binding domain from Gal4 fused to two transcription activation modules from VP16 (Asakawa et al., 2008), was expressed under the control of *pdgfrb* promoter. Exploiting these Tg lines, we demonstrated how the MCs develop and cover the ECs in the cranial and trunk vessels and identified the origins of MCs covering the cranial and trunk vasculature.

RESULTS

Development of Tg zebrafish lines for live imaging of MCs

Pdgfrb promoter is activated in MCs of mice (Foo et al., 2006). To visualize MCs using living animals, we developed *TgBAC(pdgfrb:EGFP)*, *TgBAC(pdgfrb:mCherry)* and *TgBAC(pdgfrb:Gal4FF);Tg(UAS:GFP)* zebrafish lines, in which EGFP, mCherry or Gal4FF driver was expressed under control of *pdgfrb* promoter, respectively (Fig. 1A). To simultaneously visualize the ECs and MCs, the first and the third lines were crossed with *Tg(fli1a:myryistoylation-signal tagged (Myr)-mCherry)* fish. The second line was crossed with *Tg(fli1a:Myr-EGFP)*. Expression pattern of fluorescent proteins in these reporter lines was similar to previously reported expression pattern of *pdgfrb* mRNA (Wang et al., 2014; French et al., 2014; Wiens et al., 2010). In the *TgBAC(pdgfrb:EGFP)* embryos, EGFP started to be expressed around 8-somite stage in the cranial neural crests in which *pdgfrb* mRNA is expressed (French et al., 2014) (Fig. S1A,B; Movie 1,2). EGFP expression was induced in the base of the brain from 17 h post-fertilization (hpf) (Fig. S1A,B; Movie 1,2). In the trunk of the *TgBAC(pdgfrb:EGFP)* and *TgBAC(pdgfrb:mCherry)* embryos, fluorescence signal was observed in the floor plate and hypochord at 24 hpf (Fig. S1C). At late stages, the dorsal aorta (DA), intersegmental vessels (ISVs) and dorsal longitudinal anastomotic vessels were surrounded by the EGFP-positive cells in the trunk region of *TgBAC(pdgfrb:Gal4FF);Tg(UAS:GFP)* larvae (Fig. 1B). In the head region of *TgBAC(pdgfrb:EGFP)* larvae, EGFP-positive cells covered the vessels such as central artery (CtA), basal communicating artery (BCA), posterior communicating segment (PCS), basilar artery (BA), primordial hindbrain channel (PHBC) and hyaloid vessels (HV) (Fig. 1C-E). In addition, EGFP-positive cells were accumulated in the anterior region of the DA including lateral DA where the Transgelin-

positive MCs also exist (Fig. 1F) (Santoro et al., 2009). Similarly, perivascular cells in the cranial and trunk vessels were visualized by mCherry in the *TgBAC(pdgfrb:mCherry);Tg(fli1a:Myr-EGFP)* larvae (Fig. S1D,E). These results indicate that fluorescent proteins successfully label the MCs in our reporter lines. Indeed, RT-PCR analyses revealed that EGFP-positive cells isolated from *TgBAC(pdgfrb:EGFP);Tg(fli1a:Myr-mCherry)* larvae expressed not only *pdgfrb* but also other MC marker genes such as *chondroitin sulfate proteoglycan 4* (*cspg4*) and *actin, alpha 2, smooth muscle, aorta* (*acta2*) (Fig. S1F).

We also visualized VSMCs by generating the *TgBAC(tagln:EGFP)* zebrafish line, in which EGFP is expressed under the control of smooth muscle-specific *transgelin* promoter (Robin et al., 2013). This Tg fish larvae exhibited EGFP signal in the floor plate, swim bladder, gut and rostral notochord (Fig. S1G). In addition, the EGFP-positive cells were detected in the ventral part of the DA, but not in the cranial vessels (data not shown), as previously observed in the *Tg(sm22a-b:GFP)* zebrafish line (Seiler et al., 2010). These findings indicate that the *TgBAC(tagln:EGFP)* line labels VSMCs *in vivo*.

Live imaging of MCs of blood vessels in juvenile zebrafish

Next, we investigated whether MCs can be labeled by EGFP in the juvenile *TgBAC(pdgfrb:EGFP)* zebrafish. At 1 m post-fertilization (mpf), most blood vessels in the trunk were covered by EGFP-positive cells (Fig. 1G; Fig. S1H). Blood vessels whose diameter was greater than 5-10 μm were continuously ensheathed by EGFP-positive cells and were also stained with antibody for VSMC marker, α-SMA (acta2), indicating that EGFP-positive cells were VSMCs in the *TgBAC(pdgfrb:EGFP)* zebrafish (Fig. 1G,H). Consistently, these thick vessels were also EGFP-positive in the *TgBAC(tagln:EGFP)*

zebrafish line (Fig. S1I). On the other hand, the capillaries whose diameter was less than 5 μm were irregularly and discontinuously covered by EGFP-positive cells in the *TgBAC(pdgfrb:EGFP)* fish, but not in the *TgBAC(tagln:EGFP)* line (Fig. 1G,H; Fig. S1I), suggesting that EGFP-positive cells covering the capillaries are pericytes. Thus, our *TgBAC(pdgfrb:EGFP)* line precisely monitors pericytes and VSMCs.

Live imaging of MC coverage of cranial vessels

To investigate how cranial vessels become covered by MCs, we time-lapse imaged the *TgBAC(pdgfrb:EGFP);Tg(fli1a:Myr-mCherry)* embryos, focusing on the MCs covering the CtA consisting of cerebellar CtA (CCtA), anterior mesencephalic CtA (AMCtA), middle mesencephalic CtA (MMCtA) and posterior mesencephalic CtA (PMCtA). Among them, the CCtA are formed by the ECs sprouting from the PHBC. The sprouting CCtA ECs from the PHBC first migrate dorsally to penetrate the hindbrain parenchyma, then turn ventrally and connect to the BA at 40-48 hpf (Fujita et al., 2011). During CCtA formation, weakly EGFP-positive cells existed in the cerebral base at the level of BA (Fig. 2A). Location of EGFP-positive cells implied that they might be anterior endodermal cells. However, they were not identical to *sox17* promoter-active endodermal cells (Fig. S2A). Among weakly EGFP-positive cells, the cells located in the vicinity of the BA started to emit strong green fluorescence and then made tight contact with the BA (Fig. 2A). At around 60 hpf, strongly EGFP-positive cells covering the BA started to migrate along the CCtA and frequently proliferated to cover the ECs throughout the CCtA (Fig. 2B,C; Movies 3-5). These results indicate that the CCtA is covered by the MCs that originally emerge around the BA (Fig. 2D).

MC differentiation around the BA implies an instructive role for the BA in MC

development. Consistently, the *kdr*/*kdrl*-double morphants that failed to develop the BA exhibited a lack of strongly EGFP-positive cells in the midline of the hindbrain (Fig. S2B). Although EC function is influenced by blood flow, loss of blood flow did not affect MC emergence around the BA but prevented their subsequent recruitment into the CtA (Fig. S2C). These results suggest that ECs regulate MC development independently of blood flow, while the MC recruitment might be promoted by flow-dependent EC-derived signal.

We also investigated how MCs are recruited to the AMCtA, MMCtA and PMCtA. These CtA vessels extended from the vessels located in the cerebral base such as BCA, PCS and choroidal vascular plexus (CVP) and subsequently penetrate into the brain parenchyma (Isogai et al., 2003). Weakly EGFP-positive cells located in close proximity to the BCA, PCS and CVP started to emit strong green fluorescence and were recruited to the AMCtA, MMCtA and PMCtA (Fig. S2D; Movies 4,5). By 120 hpf, most part of these CtA became surrounded by the strongly EGFP-positive cells that no longer proliferated and migrated (data not shown). Collectively, these results suggest that the CtA are covered by the MCs that originally differentiated around the vessels located in the cerebral base.

Pdgfrβ signaling is involved in recruitment and proliferation of the MCs during embryogenesis (Hellstrom et al., 1999; Olson and Soriano, 2011b; Wang et al., 2014). Thus, we analyzed the *pdgfrb*$^{sa16389/sa16389}$ mutant larvae which lack functional Pdgfrβ to clarify the role of Pdgfrβ in the MC coverage of cranial vessels (Fig. 2E; Fig. S2E). The *pdgfrb* mutant larvae normally developed cranial vessels and exhibited MC coverage of PCS, BCA and BA located in the cerebral base. However, they lost MC coverage of the CtA. Similarly, the number of MCs covering the CtA was reduced by the treatment with AG1296, a Pdgfrβ inhibitor (Fig. S2F). These results suggest that Pdgfrβ signaling is

dispensable for MC differentiation around the vessels located in the cerebral base, but indispensable for their subsequent recruitment into the CtA.

MC migration along the inter-EC junctions

We further investigated how MCs migrate along the EC tube to cover the CtA by utilizing the *Tg(fli1a:pecam1-EGFP)* line in which inter-EC junctions are visualized by Pecam1-EGFP. Time-lapse imaging revealed that MCs preferentially extended their processes along the inter-EC junctions during their migration along the CtA (Fig. 3A; Movie 6). The tip of extending process attached to the inter-EC junction in approximately 70% of the cases (Fig. S3A). In addition, approximately 60% of the total length of the processes was aligned along the inter-ECs junctions (Fig. 3B; Fig. S3B; Movie 7). Importantly, some parts of the processes spread widely on the inter-EC junctions as if the junctions became scaffold structures for the MC migration (Fig. 3C). Consistently, among 30 MCs migrating along the CtA we analyzed, 90% of them moved forward by sequentially relocating their cell bodies to the scaffold structures formed within the preceding processes (Fig. 3C; Movie 8). When the MCs migrated across the unicellular tube, they extended their processes around the EC tube even in the absence of contact with the inter-EC junctions (Fig. S3C; Movie 9). However, once the tip of processes reached to the inter-EC junctions, the MCs further extended their processes along the junctions and established the scaffold structures within these processes (Fig. S3C; Movie 9). These results suggest that during MC coverage of CtA, MCs extend their processes along the inter-EC junctions and establish the scaffold structures within the processes to move forward (Fig. 3D).

Live imaging of MC coverage of axial vessels in the trunk

Next, we analyzed MC coverage of trunk axial vessels by time-lapse imaging of the *TgBAC(pdgfrb:EGFP);Tg(fli1a:Myr-mCherry)* fish. EGFP-positive cells started to emerge in the ventral part of the DA at 36 hpf, while the posterior cardinal vein (PCV) was uncovered by EGFP-positive cells until at least 7 dpf (Fig. 4A; data not shown). Unfortunately, we could not analyze MC emergence in the dorsal side of the DA because of EGFP expression in the hypochord which was located just along the dorsal side of the DA (Fig. 4A; Fig. S1C). However, we confirmed that EGFP-positive cells in the ventral part of the DA did not originate from the hypochord. EGFP-positive cells emerged at the ventral side of the DA gradually emitted strong fluorescence and underwent cell division frequently (Fig. 4A; Movie 10). These EGFP-positive cells dorsally extended multiple processes irrespective of inter EC-junctions to ensheath the wall of DA (Fig. S4A). Proliferation of MC at the ventral part of the DA was confirmed by utilizing the Fucci (fluorescent ubiquitination-based cell cycle indicator) system (Sakaue-Sawano et al., 2008). We generated a Tg zebrafish line in which NLS-mCherry and mVenus-geminin, a Fucci biosensor for visualizing the cells in the S/G2/M phases, were simultaneously expressed in *pdgfrb* promoter-activated cells. The mCherry/mVenus double-positive cells at the ventral side of the DA apparently divided into two daughter cells, which subsequently lost mVenus fluorescence, but retained mCherry fluorescence, although these fluorescent proteins tended to be expressed in a mosaic fashion (Fig. 4B). These findings indicate that MCs cover the DA by differentiation at the ventral part of the DA and by their subsequent proliferation.

We analyzed MC coverage of the DA by utilizing the *TgBAC(tagln:EGFP)* zebrafish line to visualize the VSMCs. In the *TgBAC(pdgfrb:Gal4FF);Tg(UAS:RFP);TgBAC(tagln:EGFP)* larvae at 7 dpf, EGFP/RFP double-positive cells were observed in the ventral part of the DA (Fig. S4B,C), indicating that the MCs emerging in the ventral side of the DA were *pdgfrb*- and *tagln*-double positive VSMCs. These results were consistent with those from a previous report using a *Tg(acta2:EGFP)* line that marks smooth muscle cells (Whitesell et al., 2014). However, EGFP-positive cells at the dorsal side of the DA did not exhibit RFP expression (Fig. S4B), suggesting that VSMCs at the dorsal part do not express *pdgfrb*. Thus, distinct types of VSMCs might be present in the dorsal and ventral sides of the DA.

Live imaging of MC coverage of ISVs

We then explored when and how the ISVs become covered by MCs by analyzing the *TgBAC(pdgfrb:EGFP);Tg(fli1a:Myr-mCherry)* zebrafish. The emergence of EGFP-positive cells around the ISVs started from 48 to 60 hpf (Fig. 5A,B). The number of EGFP-positive cells in the ISVs and that of the ISVs covered by EGFP-positive cells gradually increased at least until 120 hpf (Fig. 5A,B). EGFP-positive cells tended to extend their processes along the inter-EC junctions as observed in CtA (Fig. S4D,E). However, alignment of MC processes along the inter-EC junctions in the ISVs was less frequent than in CtA, suggesting the diversity of MCs in different vascular beds. Time-lapse imaging analyses suggested two distinct modes of the MC coverage of the ISVs. One mechanism depended on recruitment of the MCs originally emerged in the ventral part of the DA. Some EGFP-positive cells located in the ventral side of the DA migrated

dorsally to cover the ISVs (Fig. 5C; Movie 10). The other mechanism involved *de novo* formation of MCs around the ISVs. Indeed, the cells located in close proximity to the ISVs started to emit green fluorescence and contacted with the ECs in the ISVs (Fig. 5D; Movie 10). Furthermore, the EGFP-positive cells around the ISVs frequently proliferated; therefore, possibly contributing to the MC coverage of ISVs (Movie 10). These results indicate that MCs cover the ISVs in two manners dependent on the recruitment of MCs from the DA and the *de novo* differentiation of MCs in the ISVs followed by their proliferation.

The number of MCs covering the ISVs increased during development (Fig. 5A). Nevertheless, approximately 40% of the ISVs remained uncovered by the MCs at 120 hpf (Fig. 5B), prompting us to hypothesize that MC coverage of the ISVs might be affected by the difference between arteries and veins. To address this hypothesis, we separately counted the number of EGFP-positive cells in the arterial ISVs (aISVs) and that in the venous ISVs (vISVs) in 120 hpf *TgBAC(pdgfrb:EGFP);Tg(fli1a:Myr-mCherry)* larvae (Fig. 5E-G). Most aISVs, but only 50% of the vISVs, were covered by the EGFP-positive cells (Fig. 5F). The number of EGFP-positive cells around the aISVs was significantly greater than that around the vISVs (Fig. 5G). These results indicate that MCs preferentially cover the aISVs comparing to the vISVs. However, despite the preferential coverage of aISVs with MCs, approximately 50% of the vISVs was also covered by the MCs (Fig. 5F). In addition, we noticed that MCs covering the vISVs tended to locate in the dorsal part (Fig. 5E,H). Since the ECs located in the dorsal part of the vISVs are thought to be derived from the DA (Isogai et al., 2003), these ECs might maintain the arterial identity even though they exist in venous vessels. If this is the case, MCs might contact with the arterial ECs within the vISVs. Therefore, we analyzed the

TgBAC(pdgfrb:EGFP);Tg(flt1:mCherry) larvae, in which arterial ECs were visualized by mCherry fluorescence (Kwon et al., 2013). Dorsal part of the vISVs was weakly but clearly labeled by mCherry fluorescence, suggesting that ECs located in the dorsal region of vISVs retain the arterial identity (Fig. 5I). Importantly, EGFP-positive cells preferentially adhered to the *flt1* promoter-activated arterial ECs comparing to the venous ECs within the vISVs (Fig. 5I,J). Taken together with the evidence that MCs covered the DA, but not the PCV (Fig. 4A), these findings indicate that arterial ECs are preferentially covered by the MCs during vascular development.

Preferential coverage of arterial ECs with MCs promoted us to hypothesize that arterial ECs might promote MC development. To test this hypothesis, we analyzed *kdrl* and *kdr* morphants that exhibited defective formation of DA and aISVs, and found that MC development in the trunk was severely impaired in the absence of DA and aISVs (Fig. S5A). These results suggest that arterial, but not venous, ECs play an instructive role in MC development. Since functional characteristics of arteries and veins partly depend on differential levels of shear stress and pressure exerted by blood flow, blood flow might be involved in MC development. However, MCs covering the DA and ISVs were observed even in the *tnnt2a* morphants that lack blood flow (Fig. S5B). Thus, arterial ECs might promote MC development in the trunk in a blood flow-independent manner.

We further investigated the role of Pdgfrβ signaling in MC development in the trunk vasculature. Neither *pdgfrb*$^{sa16389/sa16389}$ mutant nor AG1296-treated larvae showed apparent defects in trunk vessels (Fig. 5K; Fig. S5C,D). MCs covering the DA and ISVs were detected even in the *pdgfrb*$^{sa16389/sa16389}$ mutant and AG1296-treated larvae, although the number of MCs decreased comparing to the *pdgfrb*$^{sa16389/WT}$ and control larvae, respectively (Fig. 5K; Fig. S5C,D). These findings indicate that Pdgfrβ-mediated

signaling is not essential for the development of MCs covering the trunk vessels but might regulate their subsequent proliferation and recruitment.

Lineage tracing for identification of MC origins in zebrafish

The MCs originate from neural crest cells and mesoderm (Majesky, 2007; Wasteson et al., 2008; Winkler et al., 2011). To analyze the origins of MCs in the zebrafish vasculature, we established *TgBAC(pdgfrb:Gal4FF);(UAS:loxP-mCherry-loxP-mVenus)* (*pdgfrb* reporter) fish and crossed with *Tg(sox10:Cre)* (Rodrigues et al., 2012) or *Tg(tbx6:Cre,myl7:EGFP)* (Lee et al., 2013) line for labeling the neural crest- or mesoderm-derived MCs with mVenus expression, respectively (Fig. 6A). Indeed, *pdgfrb* reporter larvae crossed with *Tg(sox10:Cre)* line exhibited mVenus fluorescence in the *pdgfrb* promoter-active neural crest-derived tissues that include iris, jaw and pharyngeal arch (Mongera et al., 2013; Rodrigues et al., 2012), suggesting that this lineage tracing system works (Fig. 6B).

At first, we determined the origin of MCs in the trunk vasculature. Most MCs in the trunk vasculature were labeled with mVenus expression in the *pdgfrb* reporter crossed with *Tg(tbx6:Cre,myl7:EGFP)* line, but not in that crossed with *Tg(sox10:Cre)* line (Fig. 6B,C). To further identify the MC origin in the trunk vasculature, we analyzed the *foxd3*/*tfap2a*-double morphants which exhibited defects in neural crest formation and the *tbx6*/*hand2*-double morphants in which the tissues derived from paraxial and lateral plate mesoderm failed to develop (Lee et al., 2009; Nikaido et al., 2002; Santoro et al., 2009; Wang et al., 2011). MC emergence in the DA and ISVs was severely impaired in the *tbx6*/*hand2*-double morphant larvae but normally occurred in the *foxd3*/*tfap2a*-double morphant larvae (Fig. S6A,B). These results suggest that MCs in the trunk vessels are derived from the paraxial and lateral plate mesoderm.

Recently, Wang et al. have reported that zebrafish brain vessels contain neural crest-derived pericytes (Wang et al., 2014). However, it remains elusive whether all or specific types of brain vessels are covered by the neural crest-derived pericytes. Therefore, we addressed this question by analyzing our *pdgfrb* reporter line. When crossed with *Tg(sox10:Cre)* line, *pdgfrb* reporter fish exhibited mVenus fluorescence in the anterior part of MMCtAs and in the CVP at larval stage and in the forebrain at juvenile stage (Fig. S7A,B; data not shown). Together with the evidence that the MCs originally emerging around the CVP migrated to MMCtA (Movie 4), these results suggest that neural crest-derived MCs develop around the CVP and migrate to cover the MMCtAs. Consistently, depletion of *foxd3*/*tfap2a* led to the reduction of *pdgfrb*-positive MCs in the CVP (Fig. S7C).

In clear contrast, the mVenus-positive MCs were hardly observed in the hindbrain vessels of the *pdgfrb* reporter line crossed with the *Tg(sox10:Cre)* line (Fig. 6D; Fig. S7A,B). In addition, the MCs emerged around the BCA, PCS and BA even in the *foxd3*/*tfap2a*-double morphant larvae, although the MC coverage of CtA was significantly impaired in these morphants (Fig. S7D-F). These results suggest that neural crest cells do not contribute to the MC development in the base of hindbrain but might be required for their subsequent recruitment into the CtA.

Thus, we investigated the contribution of mesodermal cells to the MC coverage of hindbrain vasculature and found that some of the *pdgfrb* reporter larvae crossed with *Tg(tbx6:Cre,myl7:EGFP)* line showed mVenus-positive MCs in the hindbrain vessels (Fig. 6D; Fig. S7G,H). Since activity of the *tbx6* promoter used to express Cre recombinase is relatively low in the dorsal mesoderm, we also utilized the *no tail a* (*ntla*) promoter that is active in the dorsal mesoderm (Goering et al., 2003; Lee et al., 2013). In

the *pdgfrb* reporter larvae injected with a plasmid (*ntla:Cre-2A-mCherry*), mVenus-positive MCs were detected not only in the trunk vessels but also in the hindbrain vessels (Fig. S7I), suggesting mesodermal origin of MCs in the hindbrain vessels. Although we also analyzed the *tbx6*/*hand2*-double morphant larvae to confirm the mesodermal origin of MCs, they exhibited severe defects in hindbrain vessels (Fig. S7J). However, the *tbx6* morphants lacking the paraxial mesoderm-derived tissues showed decreased number of MCs covering the hindbrain vessels without apparent vascular defects (Fig. S7K-M). These results indicate that the MCs in hindbrain vessels are mainly derived from the mesoderm. In addition, lineage tracing studies and analyses of *foxd3*/*tfap2a* and *tbx6*/*hand2* double morphants revealed the neural crest origin of MCs in the hyaloid vessels (Fig. 6D;Fig. S8A,B).

Finally, we analyzed the origin of MCs covering the vessels in the pharyngeal region. mVenus-positive MCs were detected in the hypobranchial artery (HA) and aortic arches (AA) of the *pdgfrb* reporter larvae crossed with *Tg(sox10:Cre)* line, but not of those crossed with *Tg(tbx6:Cre)* line (Fig. 6E). Consistently, *foxd3*/*tfap2a*-double morphant and *foxd3* morphant larvae showed decreased number of MCs covering the HA and AA (Fig. S8C,D). These results indicate that HA and AA are covered by the neural crest-derived MCs.

DISCUSSION

In this study, we succeeded for the first time in analyzing the MC dynamics in living animals at single-cell resolution by generating the zebrafish Tg lines that express fluorescence proteins and Gal4FF driver under control of *pdgfrb* promoter. By exploiting our Tg lines, we showed that the MCs terminally differentiate around the vessels, then actively proliferate and migrate along the EC tubes, thereby covering the entire vessels. In addition, our lineage tracing analyses revealed that the MCs in the trunk vasculature are derived from the mesoderm, while those in the head region have either neural crest or mesodermal origin.

Signaling from the arterial ECs might regulate terminal differentiation of MCs. MCs mainly covered arterial blood vessels, at least, until larval stage. Similarly, preferential MC coverage of arterial vessels has been reported in mouse embryos (Hellstrom et al., 1999). Why are the arterial blood vessels mainly surrounded by the MCs? Our data showed that, although weakly EGFP-positive cells settled around both arterial and venous vessels in the *Tg(pdgfrb:EGFP)* embryos, only the cells in the close vicinity of arterial vessels were differentiated into strongly EGFP-positive MCs. In addition, MC development was impaired by the defective formation of blood vessels. These findings suggest that signaling from arterial ECs, but not from venous ECs, promotes MC differentiation. Consistently, Jagged-1, which is preferentially expressed in the arterial vessels, promotes MC differentiation through activation of Notch 3 receptors (Armulik et al., 2011; Liu et al., 2009; Villa et al., 2001).

Arterial ECs might also promote expansion of differentiated MCs surrounding the arteries. EC-derived PDGF-B is known to induce proliferation and migration of PDGFRβ-expressing MCs during embryogenesis in mice (Hellstrom et al., 1999).

Consistently, we observed that suppression of Pdgfrβ signaling inhibited MC coverage of CtA, which depends on proliferation and migration of MCs originally emerging around the vessels in the cerebral base. Importantly, since endothelial expression of PDGF-B is restricted to the arteries and capillaries in the early stage of mouse development (Hellstrom et al., 1999), arterial EC-derived PDGF-B might regulate MC coverage of arterial vessels by inducing proliferation and migration of differentiated MCs.

Coverage of the DA with VSMCs occurs through a complex mechanism. Consistent with our lineage tracing analyses, previous studies in zebrafish, quail and mice have also suggested the mesodermal origin of VSMCs in the DA (Santoro et al., 2009; Wasteson et al., 2008; Wiegreffe et al., 2007). However, VSMCs in the DA might have a heterogeneous cellular origin. At 7 dpf, *tagln*-positive cells in the ventral side of the DA were *pdgfrb*-positive, while those in the dorsal side did not express *pdgfrb*, suggesting that VSMCs in the dorsal and ventral sides of the DA have distinct origins. Consistently, it has been reported that lateral plate mesoderm-derived VSMCs cover the ventral side of the descending DA in the early stage of aortic development in mice, while the VSMCs covering the dorsal side are derived from the somites (Wasteson et al., 2008).

In zebrafish, MCs covering the cranial vessels originated from both mesoderm and neural crest cells. To date, contribution of neural crest cells to the brain MCs has been demonstrated in the vertebrates including mice, bird and zebrafish (Etchevers et al., 2001; Heglind et al., 2005; Korn et al., 2002; Trost et al., 2013; Wang et al., 2014; Yamanishi et al., 2012). Consistently, our analyses indicated the neural crest origin of MCs in the anterior part of the brain and in the hyaloid vessels. However, our data also revealed the mesodermal origin of MCs in the hindbrain vessels. Two groups have previously analyzed the origins of MCs in avian brain and have reported discrepant results. Consistent with

our observation, Etchevers et al. have reported that MCs in the forebrain are derived from neural crest cells, while those of mesodermal origin cover the vessels in the posterior part of brain (Etchevers et al., 2001). In contrast, Korn et al. have reported that neuroectoderm can give rise to the MCs in all the vessels in the brain (Korn et al., 2002). Thus, further careful examinations are required to identify the presence of mesoderm-derived MCs in the brain.

MCs migrate along the inter-EC junctions during their coverage of blood vessels. During MC coverage of CtA, the MCs extended their processes along the inter-EC junctions and subsequently relocated their cell bodies to the scaffold structures formed within the proceeding processes to move forward. It has been well-known that substrate stiffness largely influences cell migration. Indeed, recent studies have shown that many different types of cells that include VSMCs move towards stiffer substrates (Isenberg et al., 2009). Therefore, EC-EC junctions might provide a rigid scaffold required for efficient MC migration, because the inter-EC junctions are supported by the actin cytoskeleton (Ando et al., 2013; Phng et al., 2015). Alternatively, N-cadherin might regulate MC migration along the inter-EC junctions. In ECs, vascular endothelial-cadherin mediates EC-EC junctions, while N-cadherin is thought to regulate cell adhesion between the MCs and ECs. However, previous study has also reported that N-cadherin partially localizes to inter-EC junctions in addition to its plasma membrane localization (Luo and Radice, 2005). Therefore, N-cadherin expressed by the MCs might interact with N-cadherin localized at the EC-EC junctions to mediate MC migration along the inter-EC junctions. However, further studies are needed to clarify the mechanism by which MCs migrate along the inter-EC junctions and its biological significance.

Here, we have successfully uncovered the mechanism underlying MC coverage of

blood vessels by establishing novel zebrafish lines for *in vivo* visualization of MCs. Thus, Tg lines that we have developed in this study will substantially contribute to our understanding of MC biology.

MATERIAL AND METHODS

Zebrafish husbandry

Zebrafish (Danio rerio) were maintained as previously described (Fukuhara et al., 2014). Embryos and larvae were staged by hpf at 28 °C (Kimmel et al., 1995).

Image acquisition and processing

Embryos and larvae were anesthetized and mounted in 1% low-melting agarose on a 35-mm-diameter glass-base dish (Asahi Techno Glass, Shizuoka, Japan), as previously described (Fukuhara et al., 2014).

Confocal images were obtained using a FluoView FV1000 or FV1200 confocal upright microscope (Olympus, Tokyo, Japan) equipped with a water-immersion 20x (XLUMPlanFL, 1.0 NA) lens. The 473 nm, 559 nm and 633 nm laser lines were employed. Obtained confocal images were processed using Olympus Fluoview (FV10-ASW) or FluoRender (http://www.fluorender.org). Images processed with FluoRender were shown in FluoRender composite mode in which deeper objections became visible.

Fluorescence and bright field images were taken with a fluorescence stereozoom microscope (SZX12, Olympus).

Statistical analysis

Data are expressed as means ± s.e.m. Statistical significance was determined by a Student's *t* test for paired samples or one-way analysis of variance with Turkey's test for multiple comparisons. Data were considered statistically significant if P-values < 0.05.

Acknowledgements

We thank S. Schulte-Merker for providing information and plasmids for BAC recombineering, K. Kawakami for the Tol2 system and the *Tg(UAS:GFP)* and *Tg(UAS:RFP)* lines, T. J. Carney for the *Tg(tbx6:Cre,myl7:EGFP)*^{sq6} line, G. Felsenfeld for the pJC13-1 and A. Sakakibara for the iRFP670. We are grateful to M. Sone, T. Babazono, W. Koeda, K. Hiratomi and E. Okamoto for technical assistance. This work was made possible in part by software funded by the NIH: FluoRender: An Imaging Tool for Visualization and Analysis of Confocal Data as Applied to Zebrafish Research, R01-GM098151-01.

Competing interests

The authors declare no competing or financial interests.

Author Contributions

K.A., S.F. and N.M. conceived, designed the research and wrote the manuscript. K.A. performed the experiments and analyzed the results. I.N. conceived the research. H.N. and H.F. supported the experiments. R.N.H. developed *Tg(sox10:Cre)* line.

Funding

This work was supported in part by Grants-in-Aid for Scientific Research on Innovative Areas "Fluorescence Live Imaging" (No. 22113009 to S.F.) and “Neuro-Vascular Wiring” (No. 22122003 to N.M.) from The Ministry of Education, Culture, Sports, Science, and Technology, Japan, by Grants-in-Aid for Young Scientists (Start-up) (No. 26893336 to K.A.), for Scientific Research (B) (No. 25293050 to S.F. and No. 24370084 to N.M.),

and for Exploratory Research (No. 26670107 to S.F.) from the Japan Society for the Promotion of Science, by grants from the Ministry of Health, Labour, and Welfare of Japan (to N.M.); the Core Research for Evolutional Science and Technology (CREST) program of the Japan Agency for Medical Research and Development (AMED) (to N.M.); PRIME, AMED (to S.F.); Takeda Science Foundation (to S.F., N.M.); the Naito Foundation (to S.F.); Mochida Memorial Foundation for Medical and Pharmaceutical Research (to S.F.) and Daiichi Sankyo Foundation of Life Science (to S.F.). Funding for R.N.K. was provided by Medical Research Council grant MR/J001457/1.

References

Ando,K., Fukuhara,S., Moriya,T., Obara,Y., Nakahata,N., and Mochizuki,N. (2013). Rap1 potentiates endothelial cell junctions by spatially controlling myosin II activity and actin organization. *J. Cell Biol.* **202,** 901-916.

Armulik,A., Genove,G., and Betsholtz,C. (2011). Pericytes: developmental, physiological, and pathological perspectives, problems, and promises. *Dev. Cell* **21,** 193-215.

Asakawa,K., Suster,M.L., Mizusawa,K., Nagayoshi,S., Kotani,T., Urasaki,A., Kishimoto,Y., Hibi,M., and Kawakami,K. (2008). Genetic dissection of neural circuits by Tol2 transposon-mediated Gal4 gene and enhancer trapping in zebrafish. *Proc. Natl. Acad. Sci. U. S. A* **105,** 1255-1260.

Bussmann,J., Bos,F.L., Urasaki,A., Kawakami,K., Duckers,H.J., and Schulte-Merker,S. (2010). Arteries provide essential guidance cues for lymphatic endothelial cells in the zebrafish trunk. *Development* **137,** 2653-2657.

Etchevers,H.C., Vincent,C., Le Douarin,N.M., and Couly,G.F. (2001). The cephalic neural crest provides pericytes and smooth muscle cells to all blood vessels of the face and forebrain. *Development* **128,** 1059-1068.

Foo,S.S., Turner,C.J., Adams,S., Compagni,A., Aubyn,D., Kogata,N., Lindblom,P., Shani,M., Zicha,D., and Adams,R.H. (2006). Ephrin-B2 controls cell motility and adhesion during blood-vessel-wall assembly. *Cell* **124,** 161-173.

French,C.R., Seshadri,S., Destefano,A.L., Fornage,M., Arnold,C.R., Gage,P.J., Skarie,J.M., Dobyns,W.B., Millen,K.J., Liu,T., Dietz, W., Kume,T., Hofker,M., Emery,D.J., Childs,S.J., Waskiewicz,A.J., and Lehmann,O.J. (2014). Mutation of FOXC1 and PITX2 induces cerebral small-vessel disease. *J. Clin. Invest* **124,** 4877-4881.

Fujita,M., Cha,Y.R., Pham,V.N., Sakurai,A., Roman,B.L., Gutkind,J.S., and Weinstein,B.M. (2011). Assembly and patterning of the vascular network of the vertebrate hindbrain. *Development* **138,** 1705-1715.

Fukuhara,S., Zhang,J., Yuge,S., Ando,K., Wakayama,Y., Sakaue-Sawano,A., Miyawaki,A., and Mochizuki,N. (2014). Visualizing the cell-cycle progression of endothelial cells in zebrafish. *Dev. Biol.* **393,** 10-23.

Gaengel,K., Genove,G., Armulik,A., and Betsholtz,C. (2009). Endothelial-mural cell signaling in vascular development and angiogenesis. *Arterioscler. Thromb. Vasc. Biol.* **29,** 630-638.

Garg,N., Khunger,M., Gupta,A., and Kumar,N. (2014). Optimal management of hereditary hemorrhagic telangiectasia. *J. Blood Med.* **5,** 191-206.

Goering,L.M., Hoshijima,K., Hug,B., Bisgrove,B., Kispert,A., and Grunwald,D.J. (2003). An interacting network of T-box genes directs gene expression and fate in the zebrafish mesoderm. *Proc. Natl. Acad. Sci. U. S. A* **100,** 9410-9415.

Heglind,M., Cederberg,A., Aquino,J., Lucas,G., Ernfors,P., and Enerback,S. (2005). Lack of the central nervous system- and neural crest-expressed forkhead gene Foxs1 affects motor function and body weight. *Mol. Cell Biol.* **25,** 5616-5625.

Hellstrom,M., Kalen,M., Lindahl,P., Abramsson,A., and Betsholtz,C. (1999). Role of PDGF-B and PDGFR-beta in recruitment of vascular smooth muscle cells and pericytes during embryonic blood vessel formation in the mouse. *Development* **126,** 3047-3055.

Isenberg,B.C., Dimilla,P.A., Walker,M., Kim,S., and Wong,J.Y. (2009). Vascular smooth muscle cell durotaxis depends on substrate stiffness gradient strength. *Biophys. J.* **97,** 1313-1322.

Isogai,S., Lawson,N.D., Torrealday,S., Horiguchi,M., and Weinstein,B.M. (2003). Angiogenic network formation in the developing vertebrate trunk. *Development* **130,** 5281-5290.

Joutel,A., Corpechot,C., Ducros,A., Vahedi,K., Chabriat,H., Mouton,P., Alamowitch,S., Domenga,V., Cecillion,M., Marechal,E., Maciazek,J., Vayssiere,C., Cruaud,C., Cabanis,E.A., Ruchoux,M.M., Weissenbach,J., Bach,J.F., Bousser,M.G., and Tournier-Lasserve,E. (1996). Notch3 mutations in CADASIL, a hereditary adult-onset condition causing stroke and dementia. *Nature* **383,** 707-710.

Kimmel,C.B., Ballard,W.W., Kimmel,S.R., Ullmann,B., and Schilling,T.F. (1995). Stages of embryonic development of the zebrafish. *Dev. Dyn.* **203,** 253-310.

Korn,J., Christ,B., and Kurz,H. (2002). Neuroectodermal origin of brain pericytes and vascular smooth muscle cells. *J. Comp Neurol.* **442,** 78-88.

Kwon,H.B., Fukuhara,S., Asakawa,K., Ando,K., Kashiwada,T., Kawakami,K., Hibi,M., Kwon,Y.G., Kim,K.W., Alitalo,K., and Mochizuki,N. (2013). The parallel growth of motoneuron axons with the dorsal aorta depends on Vegfc/Vegfr3 signaling in zebrafish. *Development* **140,** 4081-4090.

Lee,H.C., Tseng,W.A., Lo,F.Y., Liu,T.M., and Tsai,H.J. (2009). FoxD5 mediates anterior-posterior polarity through upstream modulator Fgf signaling during zebrafish somitogenesis. *Dev. Biol* **336,** 232-245.

Lee,R.T., Knapik,E.W., Thiery,J.P., and Carney,T.J. (2013). An exclusively mesodermal origin of fin mesenchyme demonstrates that zebrafish trunk neural crest does not generate ectomesenchyme. *Development* **140,** 2923-2932.

Liu,H., Kennard,S., and Lilly,B. (2009). NOTCH3 expression is induced in mural cells through an autoregulatory loop that requires endothelial-expressed JAGGED1. *Circ. Res.* **104,** 466-475.

Luo,Y. and Radice,G.L. (2005). N-cadherin acts upstream of VE-cadherin in controlling vascular morphogenesis. *J. Cell Biol.* **169,** 29-34.

Majesky,M.W. (2007). Developmental basis of vascular smooth muscle diversity. *Arterioscler. Thromb. Vasc. Biol.* **27,** 1248-1258.

Mongera,A., Singh,A.P., Levesque,M.P., Chen,Y.Y., Konstantinidis,P., and Nusslein-Volhard,C. (2013). Genetic lineage labeling in zebrafish uncovers novel neural crest contributions to the head, including gill pillar cells. *Development* **140,** 916-925.

Nikaido,M., Kawakami,A., Sawada,A., Furutani-Seiki,M., Takeda,H., and Araki,K. (2002). Tbx24, encoding a T-box protein, is mutated in the zebrafish somite-segmentation mutant fused somites. *Nat. Genet.* **31,** 195-199.

Olson,L.E. and Soriano,P. (2011a). PDGFRbeta signaling regulates mural cell plasticity and inhibits fat development. *Dev Cell* **20,** 815-826.

Olson,L.E. and Soriano,P. (2011b). PDGFRbeta signaling regulates mural cell plasticity and inhibits fat development. *Dev. Cell* **20,** 815-826.

Phng,L.K., Gebala,V., Bentley,K., Philippides,A., Wacker,A., Mathivet,T., Sauteur,L., Stanchi,F., Belting,H.G., Affolter,M., , and Gerhardt,H. (2015). Formin-

mediated actin polymerization at endothelial junctions is required for vessel lumen formation and stabilization. *Dev. Cell* **32,** 123-132.

Robin,Y.M., Penel,N., Perot,G., Neuville,A., Velasco,V., Ranchere-Vince,D., Terrier,P., and Coindre,J.M. (2013). Transgelin is a novel marker of smooth muscle differentiation that improves diagnostic accuracy of leiomyosarcomas: a comparative immunohistochemical reappraisal of myogenic markers in 900 soft tissue tumors. *Mod. Pathol.* **26,** 502-510.

Rodrigues,F.S., Doughton,G., Yang,B., and Kelsh,R.N. (2012). A novel transgenic line using the Cre-lox system to allow permanent lineage-labeling of the zebrafish neural crest. *Genesis.* **50,** 750-757.

Sakaue-Sawano,A., Kurokawa,H., Morimura,T., Hanyu,A., Hama,H., Osawa,H., Kashiwagi,S., Fukami,K., Miyata,T., Miyoshi,H., Imamura,T., Ogawa,M., Masai,H., and Miyawaki,A. (2008). Visualizing spatiotemporal dynamics of multicellular cell-cycle progression. *Cell* **132,** 487-498.

Santoro,M.M., Pesce,G., and Stainier,D.Y. (2009). Characterization of vascular mural cells during zebrafish development. *Mech. Dev.* **126,** 638-649.

Seiler,C., Abrams,J., and Pack,M. (2010). Characterization of zebrafish intestinal smooth muscle development using a novel sm22alpha-b promoter. *Dev. Dyn.* **239,** 2806-2812.

Trost,A., Schroedl,F., Lange,S., Rivera,F.J., Tempfer,H., Korntner,S., Stolt,C.C., Wegner,M., Bogner,B., Kaser-Eichberger,A., Krefft,K., Runge,C., Aigner,L., and Reitsamer,H.A. (2013). Neural crest origin of retinal and choroidal pericytes. *Invest Ophthalmol. Vis. Sci.* **54,** 7910-7921.

Villa,N., Walker,L., Lindsell,C.E., Gasson,J., Iruela-Arispe,M.L., and Weinmaster,G. (2001). Vascular expression of Notch pathway receptors and ligands is restricted to arterial vessels. *Mech. Dev.* **108,** 161-164.

Wang,W.D., Melville,D.B., Montero-Balaguer,M., Hatzopoulos,A.K., and Knapik,E.W. (2011). Tfap2a and Foxd3 regulate early steps in the development of the neural crest progenitor population. *Dev. Biol* **360,** 173-185.

Wang,Y., Pan,L., Moens,C.B., and Appel,B. (2014). Notch3 establishes brain vascular

integrity by regulating pericyte number. *Development* **141,** 307-317.

Wasteson,P., Johansson,B.R., Jukkola,T., Breuer,S., Akyurek,L.M., Partanen,J., and Lindahl,P. (2008). Developmental origin of smooth muscle cells in the descending aorta in mice. *Development* **135,** 1823-1832.

Whitesell,T.R., Kennedy,R.M., Carter,A.D., Rollins,E.L., Georgijevic,S., Santoro,M.M., and Childs,S.J. (2014). An alpha-smooth muscle actin (acta2/alphasma) zebrafish transgenic line marking vascular mural cells and visceral smooth muscle cells. *PLoS. One.* **9,** e90590.

Wiegreffe,C., Christ,B., Huang,R., and Scaal,M. (2007). Sclerotomal origin of smooth muscle cells in the wall of the avian dorsal aorta. *Dev. Dyn.* **236,** 2578-2585.

Wiens,K.M., Lee,H.L., Shimada,H., Metcalf,A.E., Chao,M.Y., and Lien,C.L. (2010). Platelet-derived growth factor receptor beta is critical for zebrafish intersegmental vessel formation. *PLoS. One.* **5,** e11324.

Winkler,E.A., Bell,R.D., and Zlokovic,B.V. (2011). Central nervous system pericytes in health and disease. *Nat. Neurosci.* **14,** 1398-1405.

Yamanishi,E., Takahashi,M., Saga,Y., and Osumi,N. (2012). Penetration and differentiation of cephalic neural crest-derived cells in the developing mouse telencephalon. *Dev. Growth Differ.* **54,** 785-800.

Figures

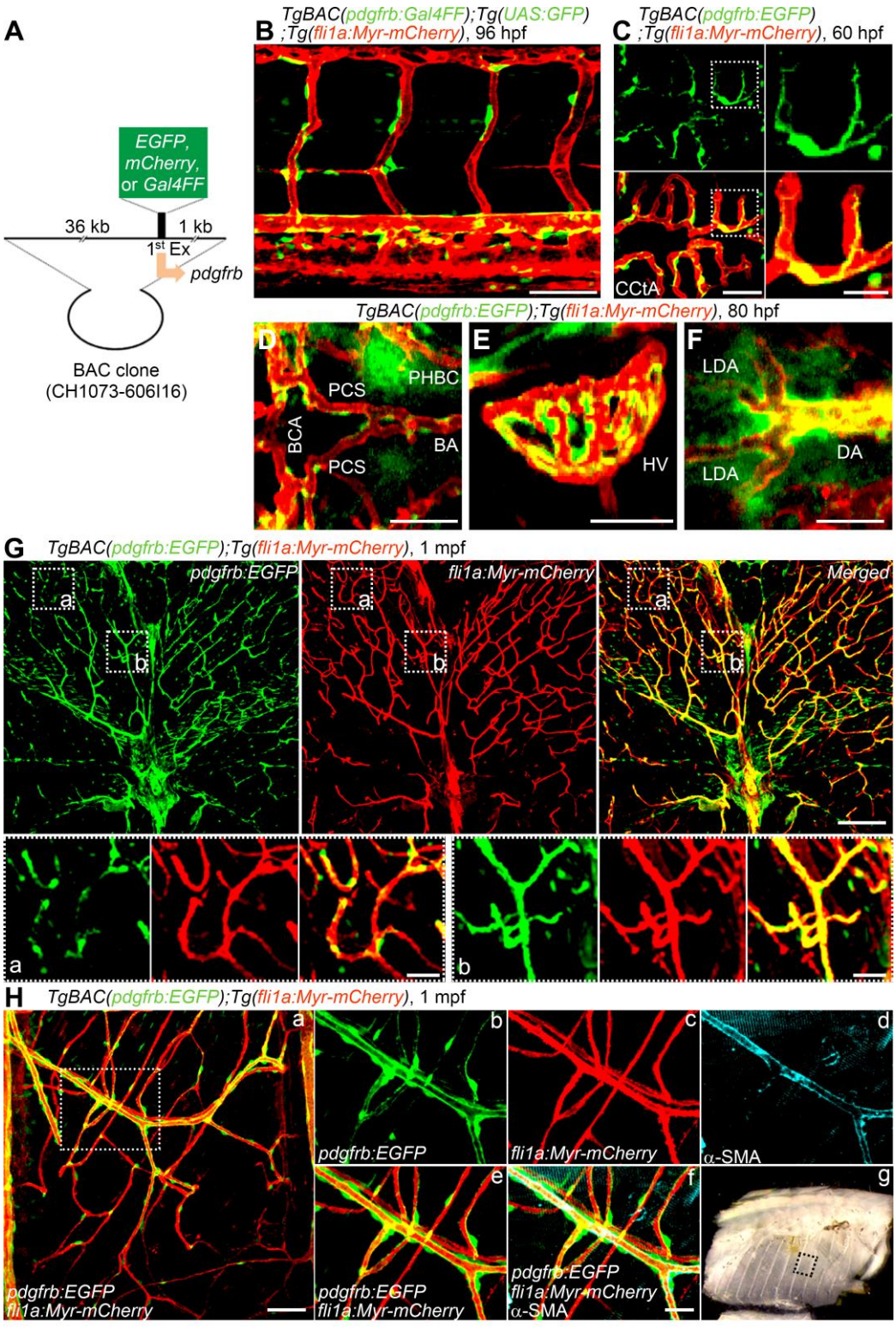

Fig. 1. Generation of Tg zebrafish lines for live imaging of MCs. (**A**) A schematic structure of a BAC clone (CH1073-606I16) used to generate Tg zebrafish lines for live imaging of MCs. A cDNA encoding either EGFP, mCherry or Gal4FF was inserted at the start codon of *pdgfrb* gene. (**B**) Confocal stack fluorescence image of trunk vasculature in the 96 h post-fertilization (hpf) *TgBAC(pdgfrb:Gal4FF);Tg(UAS:GFP);Tg(fli1a:Myr-mCherry)* larva. Lateral view, anterior to the left. The merged image of *pdgfrb:Gal4FF;UAS:GFP* (green) and *fli1a:Myr-mCherry* (red). (**C-F**) Confocal images of hindbrain vasculature (**C**, **D**), hyaloid vessels (**E**) and anterior region of dorsal aorta (**F**) in the *TgBAC(pdgfrb:EGFP);Tg(fli1a:Myr-mCherry)* larvae at 60 hpf (**C**) and 80 hpf (**D-F**). Dorsal view, anterior to the left. The merged images of *pdgfrb:EGFP* (green) and *fli1a:Myr-mCherry* (red). In **C**, the boxed areas are enlarged to the right.

(**G**) Confocal images of trunk vasculature in the 1 m post-fertilization (mpf) *TgBAC(pdgfrb:EGFP);Tg(fli1a:Myr-mCherry)* juvenile. Cross-sectional views (200 μm-thick) through the caudal region as depicted in Fig. S1H are shown. Upper left, *pdgfrb:EGFP* (green); upper center, *fli1a:Myr-mCherry* (red); upper right, the merged image. The boxed areas labeled "**a**" and "**b**" are enlarged at the bottom. (**H**) Confocal images of blood vessels in the intercostal muscle of the 1 mpf *TgBAC(pdgfrb:EGFP);Tg(fli1a:Myr-mCherry)* juvenile. Pleural tissue as indicated by the box shown in **g** was cut out and immunostained with anti-α-SMA antibody to visualize VSMC. The merged image of *pdgfrb:EGFP* (green) and *fli1a:Myr-mCherry* (red) is shown at the left (**a**). The boxed area in **a** is enlarged to the right: *pdgfrb:EGFP* (**b**), *fli1a:Myr-mCherry* (**c**), α-SMA (**d**), the merge of *pdgfrb:EGFP* (green) and *fli1a:Myr-mCherry* (red) (**e**) and the merge of *pdgfrb:EGFP* (green), *fli1a:Myr-mCherry* (red) and α-SMA (blue) (**f**). BA, basilar artery; BCA, basal communicating artery; CCtA, cerebellar central artery; DA, dorsal aorta; LDA, lateral DA; HV, hyaloid vessel; PCS, posterior communicating segment; PHBC, primordial hindbrain channel. Scale bars: 20 μm (enlarged image in **C** and **H**, **D-F**), 50 μm (**B**, **C**), 100 μm (**G**, **H**).

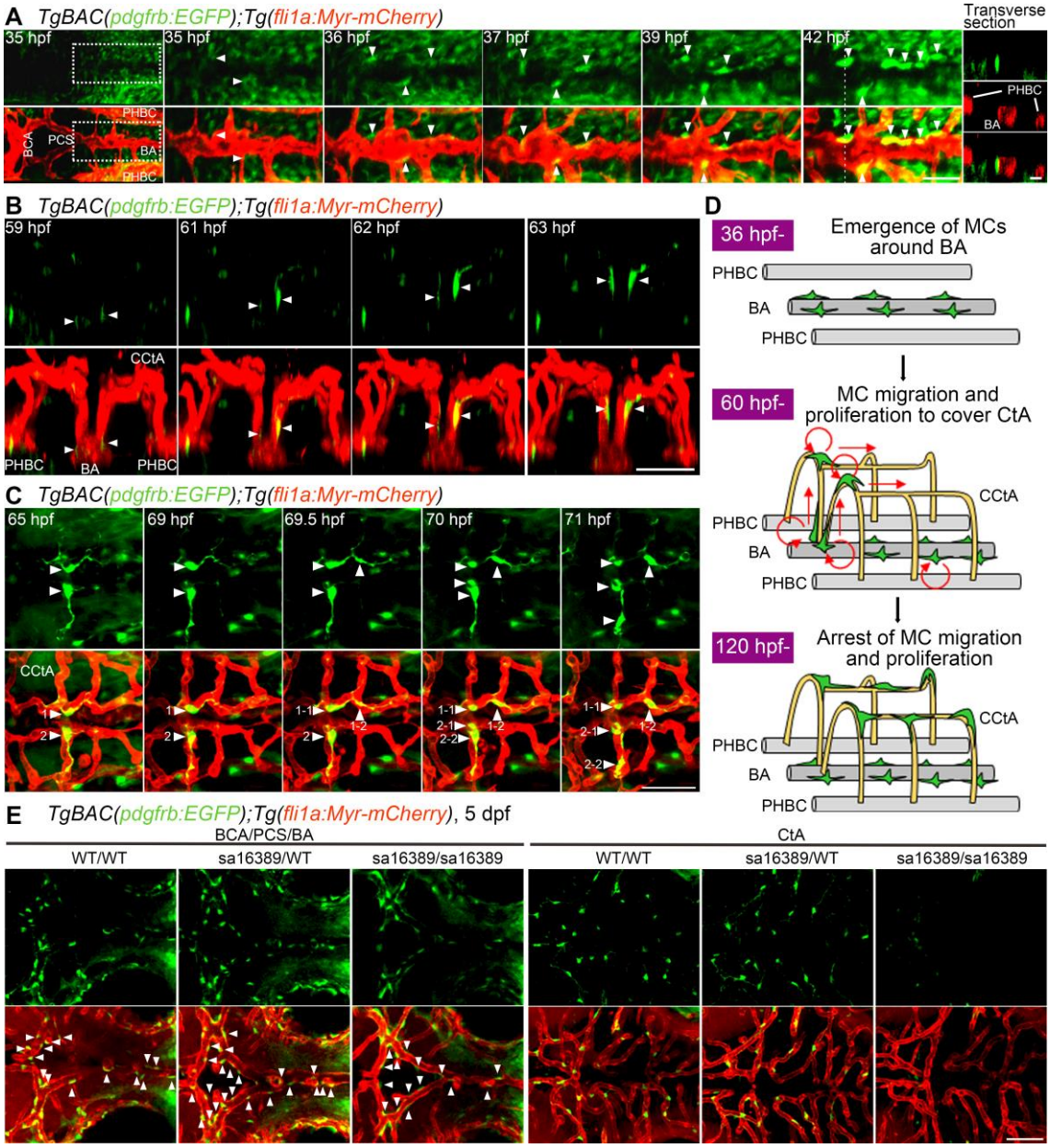

Fig. 2. Live imaging of MC coverage in cranial vessels. (**A-C**) Time-lapse confocal images of the hindbrain vasculature in the *TgBAC(pdgfrb:EGFP);Tg(fli1a:Myr-mCherry)* larvae at 35-42 hfp (**A**), 59-63 hpf (**B**) and 65-71 hpf (**C**). Upper, *pdgfrb:EGFP*; lower, the merged images of *pdgfrb:EGFP* (green) and *fli1a:Myr-mCherry* (red). (**A**) Dorsal view, anterior to the left. The enlarged images and the subsequent time-lapse images of the boxed areas in the leftmost column are shown at the right. The transverse sectional views of the areas indicated by dotted lines on the 42 hpf image are shown in the rightmost column. Top, *pdgfrb:EGFP* (green); middle, *fli1a:Myr-mCherry* (red); bottom, the merged image. Note that the cells located in the vicinity of the BA

(arrowheads) gradually emitted strong EGFP signal and tightly contacted with ECs. (**B**) 3D-rendered confocal images of EGFP-positive cells migrating along the CCtA. Lateral view, dorsal to the top and anterior to the front. Note that EGFP-positive cells locating around the BA (arrowheads) dorsally migrated along the CCtA. (**C**) Dorsal view, anterior to the left. Arrowheads with numbers indicate individual EGFP-positive cells spreading on the CCtA. Note that EGFP-positive cells spreading on the CCtA (1 and 2) divided into two daughter cells (1-1/1-2 and 2-1/2-2). (**D**) A schematic model of how CCtA become covered by MCs. MCs develop around the BA and migrate toward the CCtA. During their migration, the MCs actively proliferate to cover the CCtA. (**E**) Confocal images of hindbrain vasculature of *pdgfrb* wild type (WT/WT), heterozygous (sa16389/WT) and homozygous (sa16389/sa16389) larvae in the *TgBAC(pdgfrb:EGFP);Tg(fli1a:Myr-mCherry)* background at 5 dpf. Dorsal view, anterior to the left. The vessels in the cerebral base such as BCA, PCA and BA (BCA/PCS/BA) and the CtA are shown in the left and right columns, respectively. Upper, *pdgfrb:EGFP*; lower, the merged images of *pdgfrb:EGFP* (green) and *fli1a:Myr-mCherry* (red). Arrowheads indicate MCs emerged around the BCA, PCS and BA. Scale bars, 20 μm (transverse sectional image in **A**), 50 μm (**A**, **B**, **C, E**).

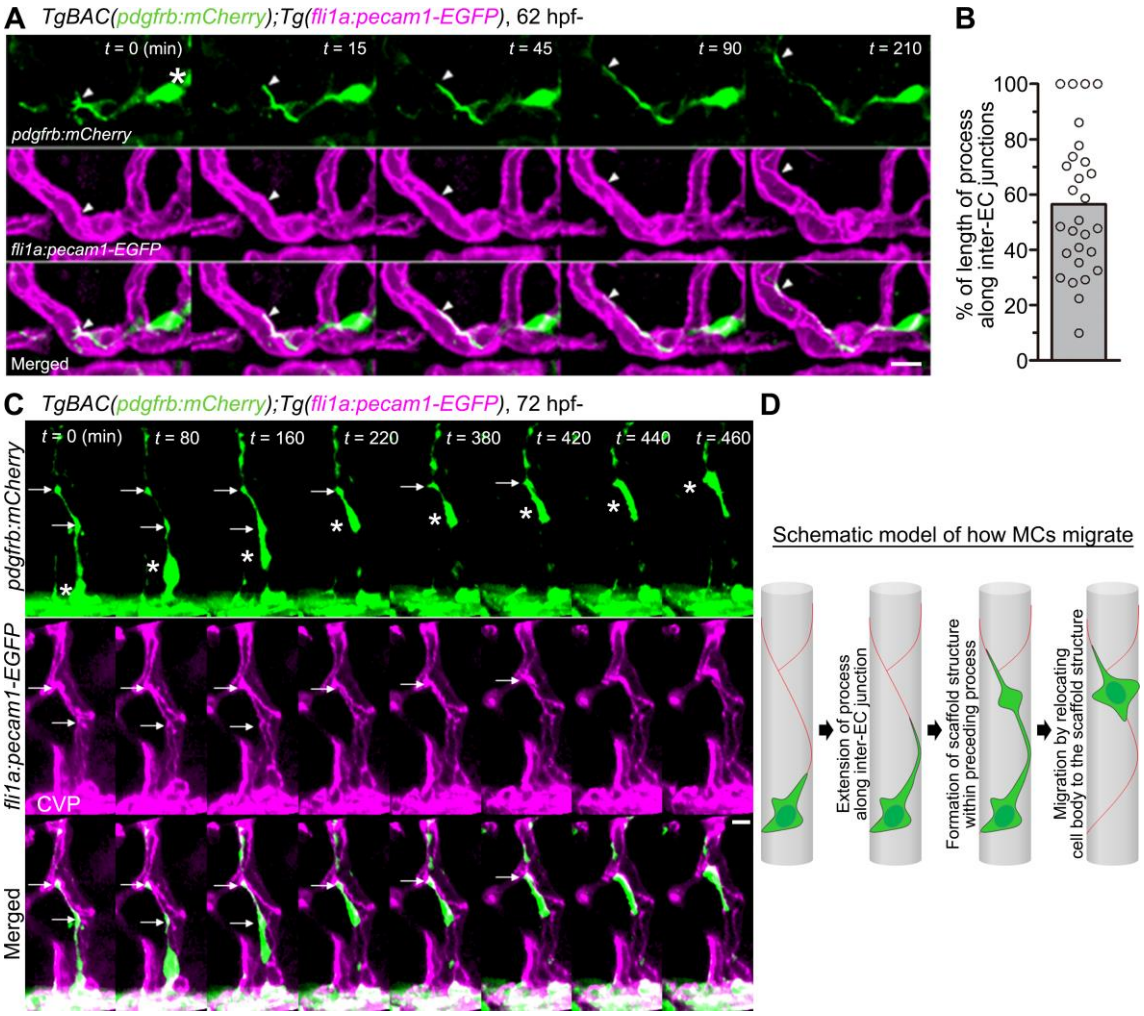

Fig. 3. Migration of MCs along the inter-EC junctions. (**A**) Time-lapse confocal images of the MC migrating along the CtA in the hindbrain of the *TgBAC(pdgfrb:mCherry);Tg(fli1a:pecam1-EGFP)* larva. The 3D-rendered confocal images at 62 hpf (leftmost column) and their subsequent time-lapse images with the elapsed time (min) at the top right. Top, *pdgfrb:mCherry* (green); middle, *fli1a:pecam1-EGFP* (magenta); bottom, the merged images. Arrowheads and asterisk indicate the tip of MC process and the cell body, respectively. Note that MC extended a process along the Pecam1-EGFP-labeled inter-EC junctions. (**B**) Alignment of MC processes along the inter-EC junctions as observed in **A** was expressed as a percentage of the total length (n = 28). Bar and circles indicate the average and the values of individual process, respectively. (**C**) Time-lapse confocal images of the MC migrating along the CtA are shown, as in **A**. 3D-rendered confocal images at 72 hpf (leftmost column) and their subsequent time-lapse images with the elapsed time (min) at the top right. Note that the MC moved forward by sequentially relocating its cell body (asterisks) to the punctate

structures formed within the preceding processes (arrows). CVP, choroidal vascular plexus. Scale bars, 10 μm (**A**, **B**). (**D**) A schematic model of how MCs migrate along the EC tube to cover the CtA. Red lines indicate the inter-EC junctions, while green cells denote MCs.

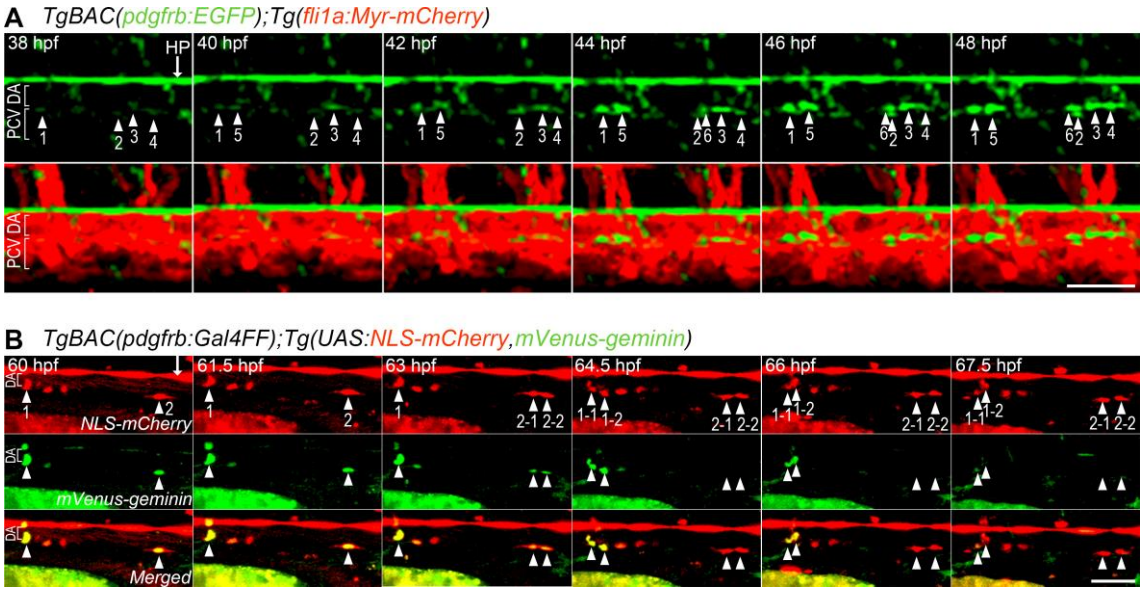

Fig. 4. Live imaging of MC coverage of axial vessels in the trunk. (**A**) Time-lapse confocal images of axial vessel in the trunk of *TgBAC(pdgfrb:EGFP);Tg(fli1a:Myr-mCherry)* embryos (38-48 hpf). Upper, *pdgfrb:EGFP*; lower, the merged images of *pdgfrb:EGFP* (green) and *fli1a:Myr-mCherry* (red). Arrowheads with numbers indicate individual EGFP-positive cells emerging at the ventral part of the DA. Arrow indicates hypochord (HP). (**B**) Time-lapse confocal images of the trunk axial vessel in *TgBAC(pdgfrb:Gal4FF);Tg(UAS:NLS-mCherry,mVenus-geminin)* embryo (60-67.5 hpf). Top, *NLS-mCherry* (red); middle, *mVenus-geminin* (the cells in the S/G2/M phase of the cell-cycle) (green); bottom, the merged images. Arrowheads with numbers indicate individual mCherry/mVenus double-positive cells located in the ventral part of DA. Note that mCherry/mVenus double-positive cells (1 and 2) divided into two daughter cells (1-1/1-2 and 2-1/2-2), which subsequently lost mVenus fluorescence. Arrow indicates hypochord. Lateral view, anterior to the left. Scale bars, 50 μm (**A**, **B**).

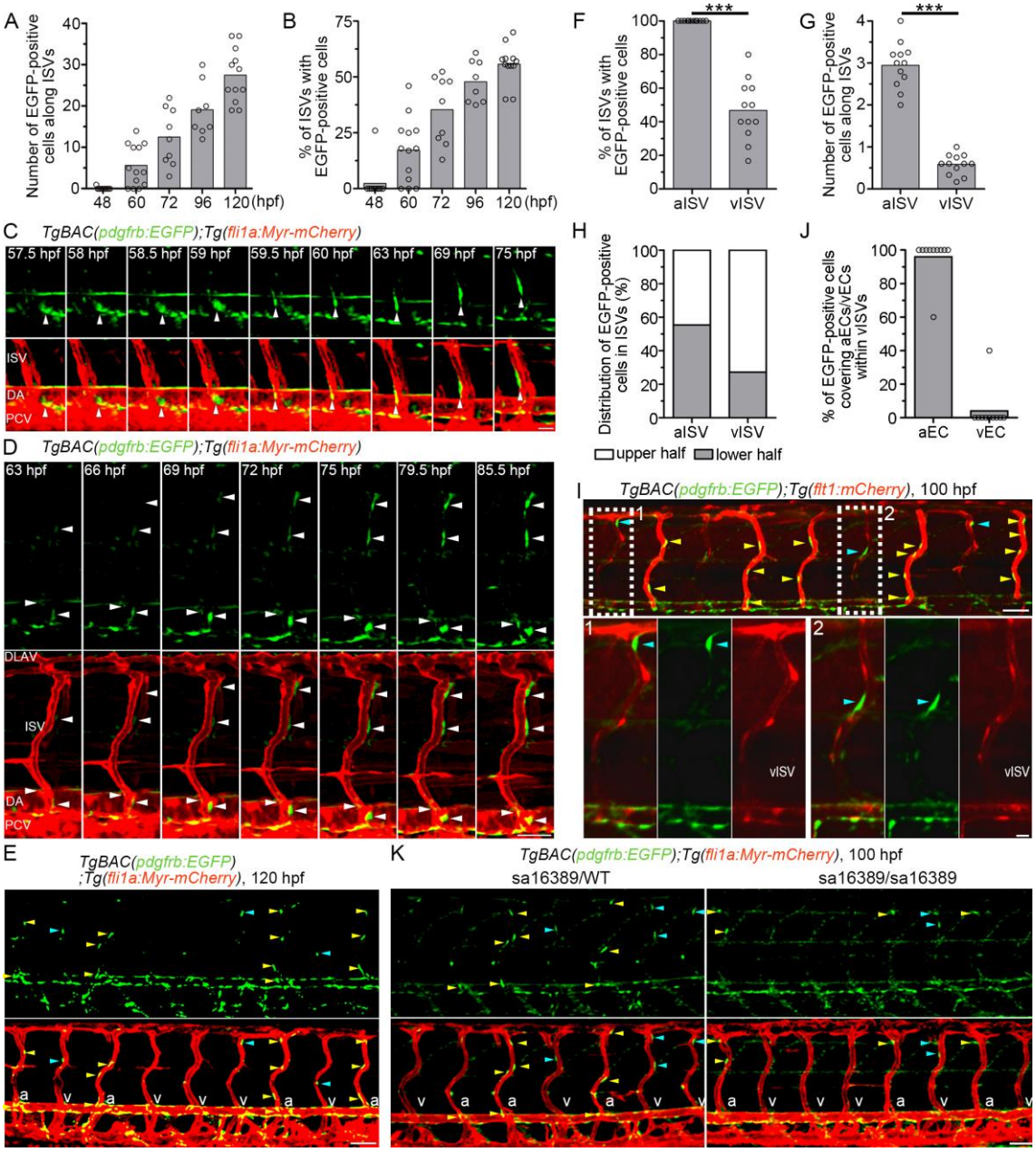

Fig. 5. Live imaging of MC coverage of ISVs. (**A**, **B**) The number of EGFP-positive cells covering mCherry-labeled ISVs (**A**) and the percentage of ISVs covered by more than 1 EGFP-positive cells (**B**) in the left side of *TgBAC(pdgfrb:EGFP);Tg(fli1a:Myr-mCherry)* embryos or larvae at the stages indicated at bottom. ($n \geq 8$). (**C**) Time-lapse confocal images of the trunk vasculature in the *TgBAC(pdgfrb:EGFP);Tg(fli1a:Myr-mCherry)* embryo (57.5-75 hpf). Upper, *pdgfrb:EGFP*; lower, the merged image of *pdgfrb:EGFP* (green) and *fli1a:Myr-mCherry* (red). Arrowheads indicate EGFP-positive cell that initially located in the ventral part of DA and subsequently migrated toward the

ISV. (**D**) Time-lapse confocal images of the trunk vasculature in *TgBAC(pdgfrb:EGFP);Tg(fli1a:Myr-mCherry)* embryo (63-85.5 hpf) are shown, as in **C**. Arrowheads indicate EGFP-positive cells covering the ISVs. Note that the cells around the ISVs gradually emitted strong EGFP signal. (**E**) Confocal images of trunk vasculature in the *TgBAC(pdgfrb:EGFP);Tg(fli1a:Myr-mCherry)* larva at 120 hpf. Upper, *pdgfrb:EGFP*; lower, the merged image of *pdgfrb:EGFP* (green) and *fli1a:Myr-mCherry* (red). Yellow and blue arrowheads indicate the EGFP-positive cells covering arterial ISVs (aISVs) and those covering venous ISVs (vISVs), respectively. "a" and "v" in the merged image indicate aISVs and vISVs, respectively. (**F**) Percentage of aISVs/vISVs covered by more than 1 EGFP-positive cell, as observed in **E**. ($n \geq 12$). (**G**) The number of EGFP-positive cells covering aISVs/vISVs, as observed in **E**. ($n \geq 12$). (**H**) Percentage of EGFP-positive cells covering the upper and lower half of aISVs/vISVs, as observed in **E**. ($n = 12$). (**I**) Confocal images of trunk vasculature in the *TgBAC(pdgfrb:EGFP);Tg(flt1:mCherry)* larvae at 100 hpf. Fluorescence signal derived from *flt1:mCherry* labels arterial ECs (Bussmann et al., 2010). The merged image of *pdgfrb:EGFP* (green) and *flt1:mCherry* (red) is shown at the top. The boxed areas labeled 1 and 2 are enlarged at the bottom, showing the merged image of *pdgfrb:EGFP* and *flt1:mCherry* (left), *pdgfrb:EGFP* (center) and *flt1:mCherry* (right). Yellow and blue arrowheads indicate the EGFP-positive cells covering aISVs and those covering vISVs, respectively. Note that MCs adhered to the *flt1:mCherry*-positive arterial ECs within vISVs. (**J**) Percentage of EGFP-positive cells adhering to arterial ECs (aEC) and those adhering to venous ECs (vECs) within vISVs, as observed in **I**. ($n = 10$). (**K**) Confocal images of trunk vasculature of the *pdgfrb* heterozygous (sa16389/WT) and homozygous (sa16389/sa16389) larvae in the *TgBAC(pdgfrb:EGFP);Tg(fli1a:Myr-mCherry)* background at 100 hpf are shown, as in **E**. In **A**, **B**, **F**, **G** and **J**, bars and circles indicate averages and each value, respectively. In **F** and **G**, ***p<0.001, significant difference between two groups. Lateral view, anterior to the left. DLAV, dorsal longitudinal anastomotic vessel ; ISV, intersegmental vessel; DA, dorsal aorta; PCV, posterior cardinal vein; aISV, arterial ISV; vISV, venous ISV. Scale bars; 20 μm (**C**, enlarged images in **I**), 50 μm (**D**, **E**, **I, K**).

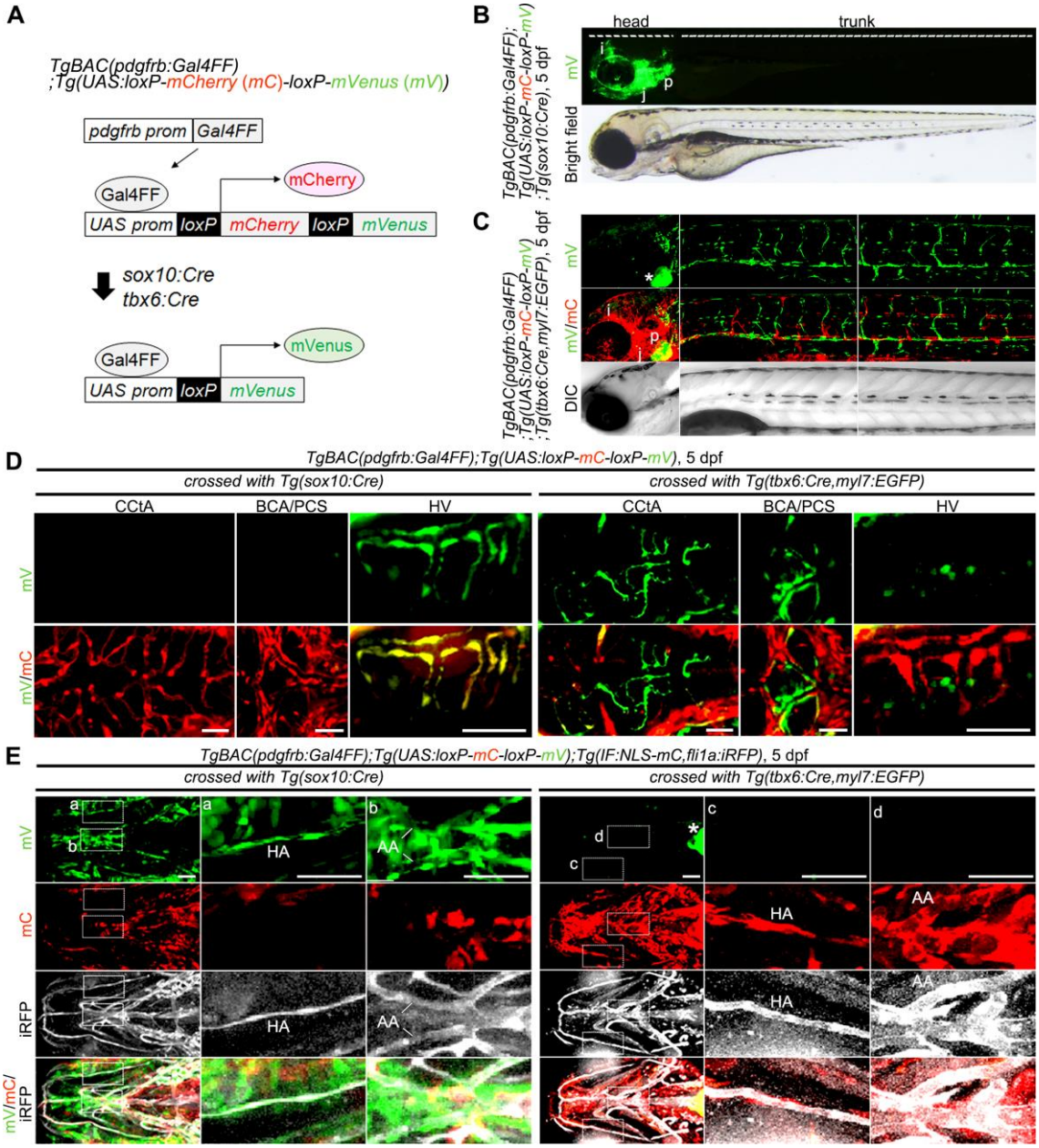

Fig. 6. Lineage tracing for identification of MC origins. (**A**) Schematic representation of the protocol used for lineage tracing analysis. *TgBAC(pdgfrb:Gal4FF);Tg(UAS:loxP-mCherry* (*mC*)*-loxP-mVenus* (*mV*)*)* zebrafish (*pdgfrb* reporter) express mCherry in the *pdgfrb*-positive cells (upper). In the *pdgfrb* reporter fish crossed with *Tg(sox10:Cre)* or *Tg(tbx6:Cre,myl7:EGFP)* line, the *sox10*-positive neural crest-derived MCs or *tbx6*-positive mesoderm-derived MCs are labeled with mVenus expression because of Cre-mediated excision of *mCherry* gene flanked by loxP, respectively (lower). (**B**) Lateral view of *TgBAC(pdgfrb:Gal4FF):Tg(UAS:loxP-mC-loxP-mV);Tg(sox10:Cre)* larva at 5

dpf. Upper, mVenus; lower, bright field image. (**C**) Confocal images of head (left column) and trunk (center and right columns) regions in the *TgBAC(pdgfrb:Gal4FF):Tg(UAS:loxP-mC-loxP-mV);Tg(tbx6:Cre,myl7:EGFP)* larva at 5 dpf. Upper, mVenus; middle, the merged images of mVenus (green) and mCherry (red); lower, differential interference contrast (DIC) images. (**D**) Confocal images of head regions in the 5 dpf *TgBAC(pdgfrb:Gal4FF):Tg(UAS:loxP-mC-loxP-mV)* larva crossed with *Tg(sox10:Cre)* (left three columns) or *Tg(tbx6:Cre,myl7:EGFP)* (right three columns) fish line. Dorsal view, anterior to the left. Images of CCtA, BCA/PCS and HV are shown in the left, center and right columns, respectively. Upper, mVenus; lower, the merged images of mVenus (green) and mCherry (red). Note that mVenus-labeled cells indicate *sox10*-positive neural crest-derived MCs (left three columns) or *tbx6*-positive mesoderm-derived MCs (right three columns). Scale bars; 50 μm (CCtA, HV), 20 μm (BCA/PCS). (**E**) Confocal images of pharyngeal regions in the 5 dpf *TgBAC(pdgfrb:Gal4FF);Tg(UAS:loxP-mC-loxP-mV);Tg(IF:NLS-mCherry,fli1a:iRFP)* larvae crossed with *Tg(sox10:Cre)* (left three columns) or *Tg(tbx6:Cre,myl7:EGFP)* (right three columns) fish line. The larvae expressing iRFP670 under the control of *fli1a* promoter was identified by *intestinal fatty acid binding protein* (*IF*) promoter-driven expression of NLS-mCherry in the intestine. Ventral view, anterior to the left. Boxed areas showing hypobranchial artery (HA) (a, c) and aortic arches (AA) (b, d) are enlarged on the right side of the original images. Top row, mVenus; 2nd row, mCherry; 3rd row, *fli1a:iRFP* (iRFP); bottom row, the merged images of mVenus (green), mCherry (red) and iRFP (white). Scale bars, 50 μm. Asterisks in **C** and **E** indicate heart visualized by *myl7:EGFP*. mC; mCherry, mV; mVenus, i; iris, j; jaw, p; pharyngeal arch.